Electrochimica Acta 66 (2012) 94–99

Contents lists available at SciVerse ScienceDirect

Electrochimica Acta

journal homepage: www.elsevier.com/locate/electacta

Direct measurement of lithium transport in graphite electrodes using neutrons

Jon P. Owejan[a,*], Jeffrey J. Gagliardo[a], Stephen J. Harris[a], Howard Wang[b], Daniel S. Hussey[c], David L. Jacobson[c]

[a] General Motors Electrochemical Energy Research Laboratory, 10 Carriage Street, Honeoye Falls, NY 14472, USA
[b] Department of Mechanical Engineering, State University of New York at Binghamton, 4400 Vestal Parkway East, Binghamton, NY 13902, USA
[c] National Institute of Standards and Technology, Physical Measurement Laboratory, 100 Bureau Drive, Gaithersburg, MD 20899, USA

ARTICLE INFO

Article history:
Received 1 November 2011
Received in revised form 12 January 2012
Accepted 13 January 2012
Available online 30 January 2012

Keywords:
Lithium
Battery
Intercalation
Graphite
Transport
Neutron

ABSTRACT

Lithium intercalation into graphite electrodes is widely studied, but few direct in situ diagnostic methods exist. Such diagnostic methods are desired to probe the influence of factors such as charge rate, electrode structure and solid electrolyte interphase layer transport resistance as they relate to lithium-ion battery performance and durability. In this work, we present a continuous measurement of through-plane lithium distributions in a composite graphite/lithium metal electrochemical cell. Capacity change in a thick graphite electrode was measured during several charge/discharge cycles with high resolution (14 μm) neutron imaging. A custom test fixture and a method for quantifying lithium are described. The measured lithium distribution within the graphite electrode is given as a function of state of charge. Bulk transport resistance is considered by comparing intercalation rates through the thickness of the electrode near the separator and current collector. The residual lithium content associated with irreversible capacity loss that results from cycling is also measured.

© 2012 Elsevier Ltd. All rights reserved.

1. Introduction

The application of lithium-ion batteries in electric vehicles is challenged by durability. Scaling this technology from its origins in consumer electronics has highlighted significant aging issues that are outside the typical useful life of small and inexpensive devices. In automotive applications, the capacity fade observed with typical materials used in large scale Li-ion batteries is unacceptable from both a customer satisfaction and warranty cost standpoint relative to the current internal combustion engine paradigm. Loss of capacity over time is related to electrolyte decomposition, active material dissolution, phase change in the insertion electrodes and passivating film formation [1]. Mobile lithium lost in the growth of the solid electrolyte interphase (SEI) layer on electron conducting surfaces encapsulates several of these mechanisms [2]. As this layer becomes thicker, increased Li-ion transport resistance will further decease performance [3].

Throughout the years of lithium battery research, many mathematical models describing the distributed multi-scale transport physics of lithium ions have been proposed [4–6]. These modeling approaches are constantly being updated based on the evolving knowledge of material interactions and the impact of cycling parameters. On the experimental side, many of these insights come from numerous spectroscopy techniques, light absorption, NMR or from electrochemical measurements which include cyclic voltammetry, potentiostatic/galvanostatic intermittent titration techniques (P/GITT), and electrochemical impedance spectroscopy (EIS). Combined, these techniques are being used to fundamentally describe Li-ion transport in the liquid electrolyte and insertion processes in the intercalation electrodes with SEI layer interactions [2,7].

Direct measurement of in situ lithium mobility with improved spatial resolution is required for validation of these increasingly complicated models. In graphitic negative electrodes, researchers have utilized the colorimetric response of the various phases of lithium insertion into carbon [8–10]. These mesoscale surface measurements provide time resolved lithium transport and insertion rates at a state of charge (SOC) between 50% and 100%. Performing continuous charge/discharge cycles enables one to measure changes in Li-ion diffusion resistance and heterogeneity in charge distribution. Below 50% SOC there is not a significant color change to measure; this combined with the in-plane nature of this experiment limits the user's ability to study the loss of lithium and the impact of charging rate.

Neutron radiography has also been considered for direct measurements of Li-ion transport in batteries due to the large neutron cross-section associated with the isotope ^{6}Li. Early work applying this technique ultimately demonstrated optical contrast in typical intercalation electrodes varied with SOC [11,12]. This research was expanded to consider electrolyte consumption and gas evolution

* Corresponding author. Tel.: +1 585 953 5558; fax: +1 585 624 6680.
E-mail address: jon.owejan@gm.com (J.P. Owejan).

0013-4686/$ – see front matter © 2012 Elsevier Ltd. All rights reserved.
doi:10.1016/j.electacta.2012.01.047

[13,14]. Recent improvements in detector spatial and temporal resolution have enabled tomographic studies of commercial can cells [15,16] and real-time monitoring of anode vs. cathode lithium content in pouch cells [17]. Although quantitative measurement of Li content is feasible with neutron radiography, to date no reported research has done so. To maximize the utility of this measurement technique, lithium transport must be quantified real-time in the through-plane dimension of typical electrode materials.

A battery test fixture, specifically designed for high resolution neutron imaging was developed for the current study. With this fixture, lithium intercalation in a composite graphite electrode is measured for several galvanostatic charge/discharge cycles. An on-line lithium calibration method based on capacity change monitored electrochemically is presented and theoretical uncertainty in the associated lithium content is also described. For a typical graphite electrode, these experiments identify heterogeneous lithium distributions during discharge, lost lithium as a function of cycling, and future challenges associated with quantification in practical materials.

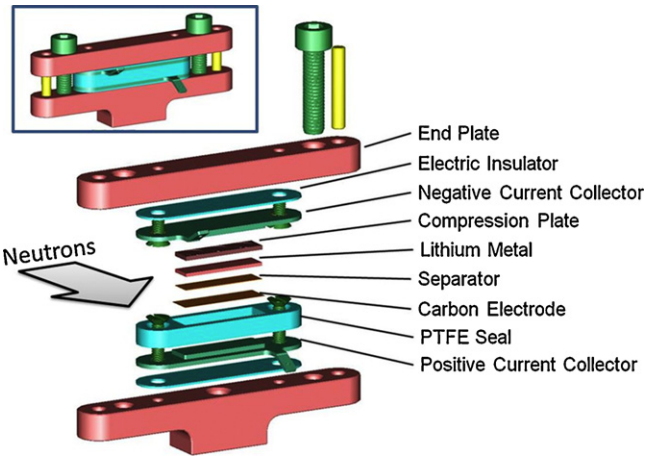

Fig. 1. Battery test fixture for high resolution neutron imaging of transient lithium content.

2. Experimental

This experimental campaign was designed to evaluate the utility of neutron imaging for measuring lithium intercalation rates and associated heterogeneities two-dimensionally in the through-plane dimension of an intercalation electrode. Experiments were executed with discharge (lithiation of graphite)/charge (delithiation of graphite) cycles at a C/9 C-rate (where 1 C-rate is the required current to discharge the theoretical capacity in 60 min.) between 2.0 and 0.007 V vs. Li with simultaneous neutron imaging. The three key unique components of these experiments are the neutron radiography method, lithium calibration and battery test fixture.

2.1. Neutron radiography

Neutron imaging has been successfully applied for liquid water mapping and quantification in proton exchange membrane fuel cells by many researchers, these methods were reviewed by Trabold et al. [18]. Procedures for quantifying lithium are analogous to liquid water, with added uncertainty associated with changes in the electrolyte composition, gas evolution, and residual lithium that results from SEI layer growth or plating. Unlike a fuel cell, the reference state of a battery is constantly changing. To account for these changes, a reference at the fully charged state between cycles is used for analysis of lithium insertion rates and these reference states were also compared to consider trapped lithium content as a function of cycling.

The neutron radiography was performed at the National Institute of Standards and Technology (NIST) research reactor with the Neutron Imaging Facility. The 1 cm shutter and 0.1 cm × 1.0 cm aperture used provides a neutron fluence rate of 6.54×10^5 neutrons cm^{-2} s^{-1} [19]. The length to aperture ratio is 6000 × 600 (through-plane by in-plane dimension) with the detector located $L = 6$ m from the aperture. The NIST micro-channel plate detector used in these experiments has a resolution of 13 μm, and the through-plane geometric blur is less than 5 μm given the maximum sample distance from the detection plane [20].

Reference and in situ battery experiment images were counted for 5 min then averaged in groups of 10. This analysis resulted in 50 min time averaged arrays with an average of 5 counts per pixel. These poor counting statistics highlight the need for fully deuterated electrolyte and minimized integration distance. The integrated lithium content, regardless of phase in the graphitic electrode was calculated based on the initial charged state with intensity I_{ref} per Eq. (1). Here, the neutron contrast is represented by I_{Li}/I_{ref} where I_{Li} is the intensity during intercalation and this ratio is also monitored and corrected for variation in neutron fluence from the reference image and background gamma noise.

$$I_{Li} = I_{ref} e^{-\mu_{Li} t_{Li}} \quad (1)$$

2.2. Li half cell test fixture

Button-type battery test cells are not optimal for through-plane neutron imaging. The circular geometry complicates the analysis and introduces more geometric blur for a given active area. Additionally, the stainless steel casing is not an ideal material for neutron transmission. To address these issues, a fixture was specifically designed with rectangular active geometry and a neutron transparent polytetraflouroethylene (PTFE) casing. Shown in Fig. 1, the 5 mm × 15 mm active area of this design enabled a minimized detection distance with a simple geometry along the path of integration which resulted in a maximum sample distance from the detector of 1.3 cm.

For the image spatial resolution of 14 μm (with geometric blur of 5 μm), the lithium content as a function of electrode depth requires a thicker intercalation electrode. Typical graphite composite electrodes of 50 μm thickness would yield insufficient measurement points across the thickness to provide insight regarding Li distributions. To improve these measurement statistics and observe trends through the thickness of the electrode during charge/discharge cycling, a 300 μm thick electrode was used. This electrode consisted of 90% Timrex[1] SLP30 graphite active material (tap density of 0.79 g/ml), 6% Timcal Super P Li conductivity enhancer, and 4% Kynar HSV900 (Arkema) binder by weight. The electrolyte was 1 M $LiPF_6$ in 1:2 (v/v) deuterated ethylene carbonate (EC):protonated diethyl carbonate (DEC). Partially deuterated solvent was used to improve neutron contrast. The half cell assembly was completed with a 750 μm natural Li foil counter electrode and a 25 μm Celgard series 2500 separator.

[1] Certain trade names and company products are mentioned in the text or identified in an illustration in order to adequately specify the experimental procedure and equipment used. In no case does such identification imply recommendation or endorsement by the National Institute of Standards and Technology, nor does it imply that the products are necessarily the best available for the purpose.

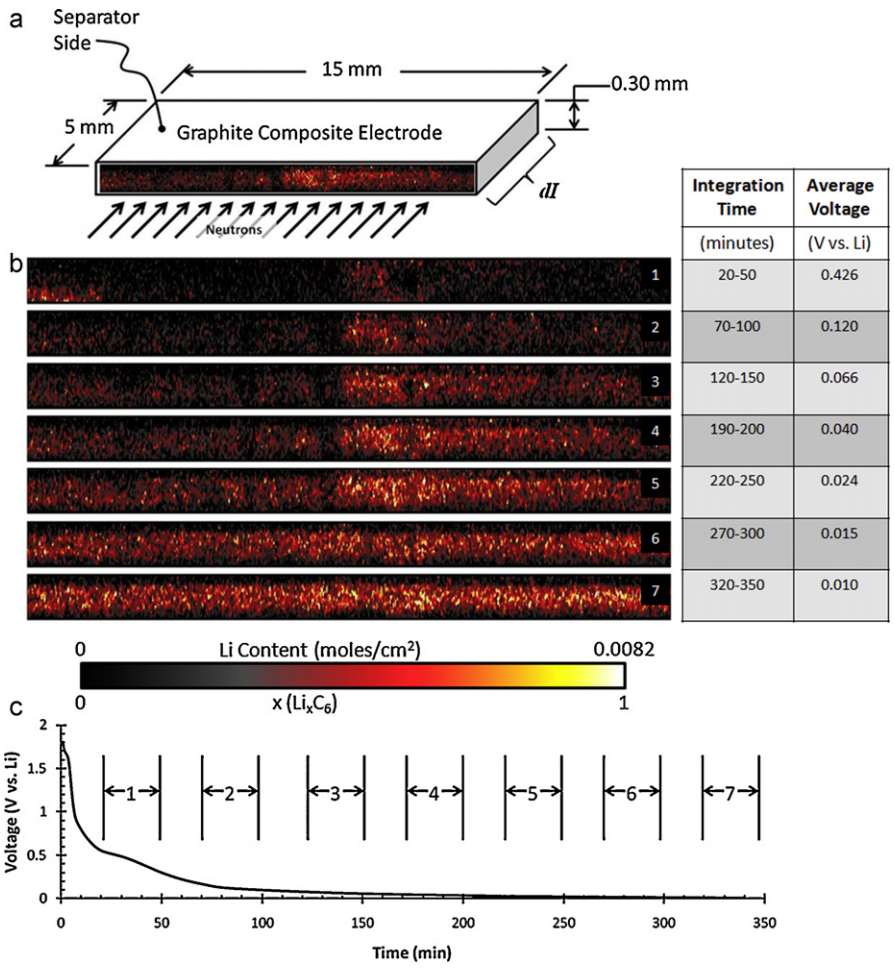

Fig. 3. Lithium distributions in composite graphite electrode during the first discharge, (a) geometry of test setup, (b) time resolved radiographs, (c) voltage response at C/9 discharge rate.

2.3. Quantifying lithium content

From Eq. (1), the natural logarithm of I_{Li}/I_{ref} is proportional to the integrated lithium content, which is equated to a macroscopic neutron cross-section (μ_{Li}) multiplied by the material thickness (t_{Li}). By doing these experiments with simultaneous neutron and electrochemical data collection, an on-line lithium calibration can be executed to quantify lithium being inserted into the system rather than using a calibration standard. The sum of the attenuation change for the entire electrode is assumed to be associated only with lithium insertion by equating all charge transfer to the half cell reaction:

$$xLi^{+} + xe^{-} + 6C \leftrightarrow Li_xC_6 \tag{2}$$

Hence, every lithium atom corresponds to one electron in the galvanostatically controlled charge/discharge cycles. This is valid because neutrons are sensitive to the number density of lithium nuclei, not material density. Because all SEI components contain lithium, this assumption does not add uncertainty regarding the passivation layer. From electrochemical data, the total moles of lithium (n_{Li}) transferred is given by the charge divided by the elemental charge and Avogadro's number. Reordering Eq. (1), summing over the entire electrode pixel array (P_x, P_y) and normalizing by the cross-sectional area (A) of the electrode results in μ_{Li} equal to:

$$\mu_{Li} = -\frac{A}{n_{Li}} \ln\left(\frac{\Sigma_i^{P_x}\Sigma_j^{P_y} I_{Li}[i,j]}{\Sigma_i^{P_x}\Sigma_j^{P_y} I_{ref}[i,j]}\right) \tag{3}$$

The result of this calibration for 4 discharge cycles is shown in Fig. 2, where a linear fit forced through the origin resulted in μ_{Li} = 18.2 cm^2/mole with a standard deviation of 1.5 cm^2/mole. This value, measured for the entire electrode, was used at the pixel level to quantify distributed lithium content. Equating this calibration to equivalent units of a scattering cross section results in 30.2 barns whereas the published value is 71.9 barns [21]. This significant difference is likely related to a number of factors, including electrode swelling, beam hardening, spatial resolution, etc. which are similar to systematic effects identified in imaging hydration of proton exchange membranes [20]. The fundamental nature of this difference will be the subject of further investigation, however, for the purpose of the current study, we believe that the on-line calibration accounts for these effects. This method of calibration also eliminates several other uncertainties associated with an offline calibration. Fixture effects, changes in electrolyte composition, and a precise reference value of lithium in the electrode were captured with this method.

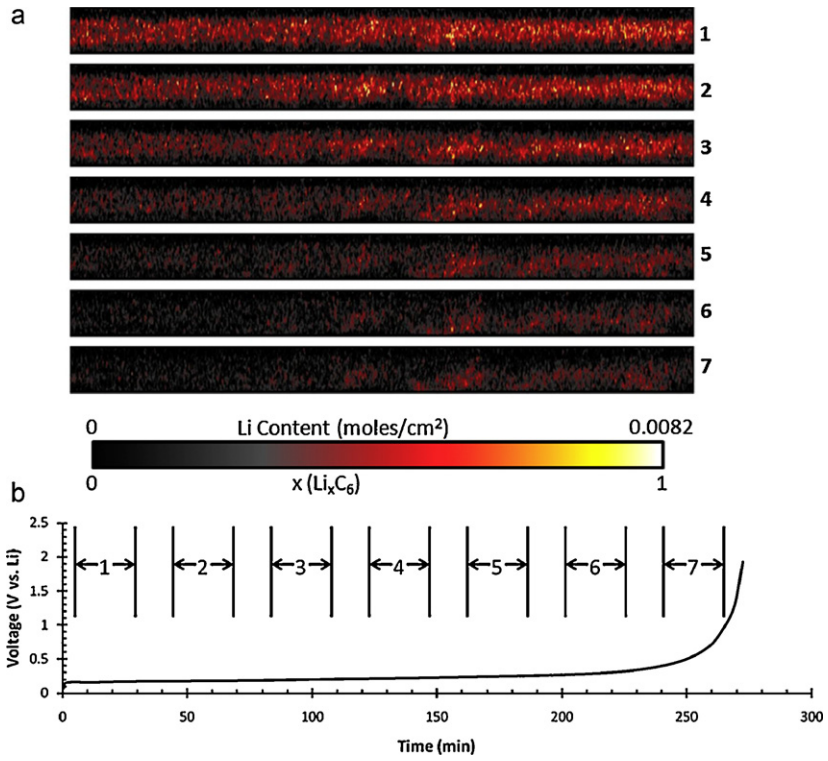

Fig. 4. Lithium distributions in composite graphite electrode during the first charge, (a) time resolved radiographs, (b) voltage response at C/9 charge rate.

3. Results

A series of normalized radiographs at averaged time intervals during the first discharge are shown in Fig. 3. The intensity plots represent the total lithium content integrated through the electrode width. Based on the known active carbon content in the electrode, the stage (x) from the half cell reaction is equated to the moles/cm^2 scale in Fig. 3 where the active carbon mass was 266 mg which corresponds to maximum lithium content of $3.7e^{-4}$ moles when $x = 1$, or 0.0082 moles/cm^2 if normalized by area. When comparing the lithium distributions at different points in time during the discharge, it is observed that the initial lithium distribution is highly nonuniform, especially along the electrode length where a discontinuity in lithium concentration forms near the center. Nearer to the end of the discharge this distribution is shown to relax, becoming more uniform throughout the electrode. The initial distribution is likely caused by trapped gas or inhomogeneities in the electrode structure; however these effects cannot be directly quantified with this through-plane setup but has been shown to be significant with previous in-plane work by Goers et al. [14]. The subsequent charge shown in Fig. 4 indicates the delithiation process is more uniform across the electrode length, perhaps a result of the relaxation that occurred at the end of the previous discharge.

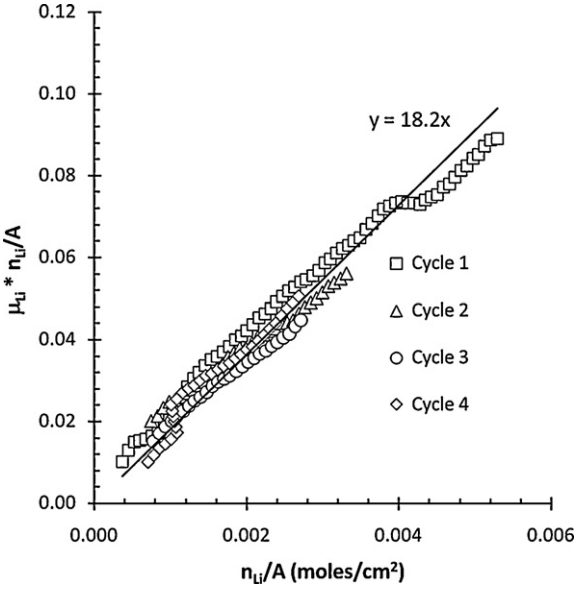

Fig. 2. Attenuation coefficient (Eq. (3)) measured based on intensity change for entire electrode cross-sectional area compared lithium content measured in a constant current discharge.

A gradient in the average through-plane distribution (depth of the electrode) is also observed in Figs. 3 and 4. This gradient is considered quantitatively for the first discharge in Fig. 5, where the lithium content in (70 ± 7) μm of electrode thickness near both the separator and current collector are averaged across the entire electrode length and plotted against discharge time. These 70 μm sections compared in Fig. 5 represent an average 170 μm transport distance in the depth of the electrode. Clearly the lithium insertion rate near the separator is faster than near the current collector. A linear model of these data was used to approximate this increase in transport resistance. For the 170 μm through-plane electrode transport length, the solid-state diffusion rate decreased by 27%, and this reduction was confirmed to scale proportionally with depth. A similar transport resistance was also calculated for the delithiation process during charging. Thus, for a typical 50 μm negative graphite composite electrode, these results indicate bulk transport resistance in the depth of the electrode is small at beginning of life and a low C-rate of C/9. However, for the thick electrode used in this experiment it contributes to the poor faradaic yield given in Fig. 6 (relative to the theoretical specific reversible charge of 372 mAh/g for graphite). In the current configuration,

concentration gradients in the electrolyte only have a small signal relative to lithium in graphite and this is lumped into the overall measurement, thereby prohibiting conclusions regarding the ionic concentration changes in the depth of the electrode that cause the slower solid-state diffusion. It should also be noted that this electrode was not optimized through modifications in the formulation to improve ionic transport resistance for high capacity storage.

Subsequent cycling of the battery revealed the absolute content of lithium measured with neutron imaging was increasing beyond the electrochemically measured capacity. Using the virgin electrode image as a reference for these cycles, this was found to be a result of the electrode lithium content not returning to a near zero value after the charge step. This effectively counts trapped lithium from the previous discharge cycle. By comparing the virgin electrode to the fully charged state of each cycle, the residual lithium can be determined and is given in Fig. 6. These residual

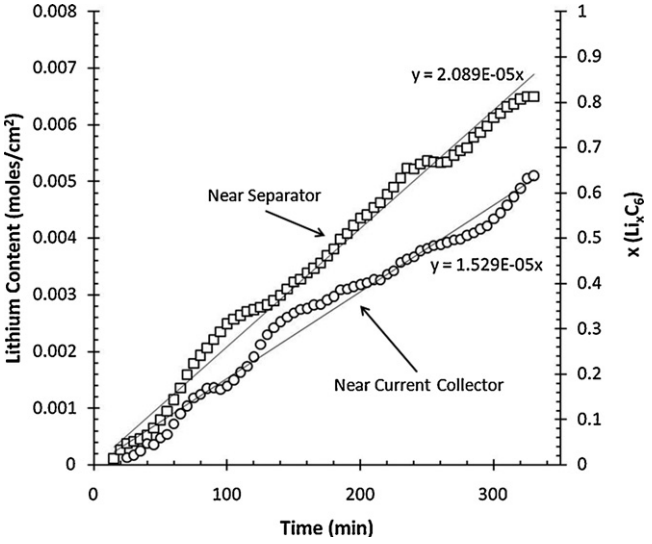

Fig. 5. Lithium insertion measured with neutron radiography near the separator and current collector, averaged across the electrode length for two 70 μm differential electrode thicknesses that are 170 μm apart with respect to the depth of the electrode.

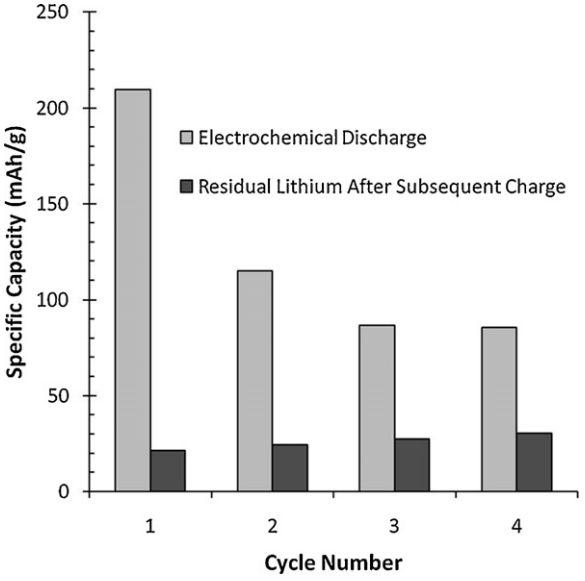

Fig. 6. Specific capacity measured electrochemically for entire discharge and cumulative irreversible capacity loss associated with residual lithium at a fully charged state measured with neutrons.

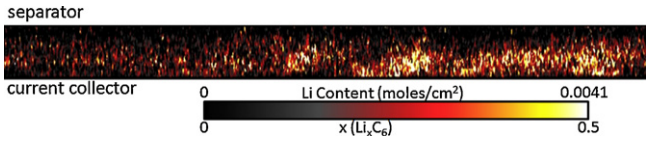

Fig. 7. Residual lithium distribution at fully charged state after the first discharge/charge cycle.

values were subtracted in the original calibration such that both the electrochemical and neutron data used in Fig. 3 started from a new zero value for direct comparison.

In a practical system with a finite lithium source these residual values would represent irreversible capacity loss associated with immobile lithium in the graphite electrode or as components of the SEI layer. To estimate the relative influence of the SEI layer lithium content, a simple calculation of a 100 nm lithium layer covering the entire electrode surface area reveals that even in this conservative scenario the contribution of SEI components is negligible relative to the total measured residual content. Therefore, it is likely that the cumulative residual lithium shown in Fig. 6 is trapped in the bulk electrode material. This distribution is given in Fig. 7 where the majority of trapped lithium is concentrated near the current collector side of the electrode and by comparing this to Fig. 3 it is observed that the residual content correlates to regions with low intercalation rates observed in the first lithiation cycle. This suggests that lost lithium is linked to regions with higher local transport resistance.

4. Conclusions and future work

Lithium transport in intercalation electrodes has been quantified with neutron radiography using an on-line calibration. Spatiotemporal measurements through the electrode thickness during galvanostatic cycling with high resolution neutron imaging revealed a nonuniform lithium concentration distribution existed early in the intercalation cycle at low C-rate but relaxed to a more homogeneous distribution at low potentials. Comparing intercalation rates near the separator and current collector indicated a small but measurable through-plane transport resistance existed in the bulk of the graphite composite electrode. By cycling the battery and comparing the lithium content at a fully charged state, the distribution of lost capacity associated with trapped lithium was quantified. In future work we will consider thinner electrodes and the systematic effects of material changes in the battery resulting from gas evolution, electrode expansion, and composition changes in the electrolyte on measurement uncertainty. We will also continue investigating calibration methods with off-line lithium metal and lithium-containing materials of known thicknesses. The ultimate goal of the continuing work is to enable durability experiments that directly measure the capacity fade in Li-ion battery electrodes spatiotemporally. This technique will also be useful for the evaluating control strategies to manipulate residual lithium.

Acknowledgements

This work was supported by NIST ARRA grant number 60NANB10D027. The authors thank Jeanette Owejan, Matthew Dioguardi, and Robert Moses from the General Motors Electrochemical Energy Research Lab; and Eli Baltic from the NIST Physical Measurement Lab.

References

[1] P. Arora, R.E. White, M. Doyle, J. Electrochem. Soc. 145 (1998) 3647.
[2] K. Xu, Chem. Rev. 104 (2004) 4303.
[3] J. Christensen, J. Newman, J. Electrochem. Soc. 150 (2003) A1416.

[4] M. Doyle, T. Fuller, J. Newman, J. Electrochem. Soc. 140 (1993) 1526.
[5] G.G. Botte, V.R. Subramanian, R.E. White, Electrochim. Acta 45 (2000) 2595.
[6] S. Santhanagopalan, Q. Guo, P. Ramadass, R.E. White, J. Power Sources 156 (2006) 620.
[7] D. Aurbach, M.D. Levi, E. Levi, Solid State Ionics 179 (2008) 742.
[8] P. Maire, A. Evans, H. Kaiser, W. Scheifele, P. Novak, J. Electrochem. Soc. 155 (2008) A862.
[9] S.J. Harris, A. Timmons, D.R. Baker, C. Monroe, Chem. Phys. Lett. 485 (2010) 265.
[10] P. Maire, H. Kaiser, W. Scheifele, P. Novák, J. Electroanal. Chem. 644 (2010) 127.
[11] M. Kamata, T. Esaka, S. Fujine, K. Yoneda, K. Kanda, J. Power Sources 68 (1997) 459.
[12] T. Esaka, Ionics 10 (2004) 358.
[13] M. Lanz, E. Lehmann, R. Imhof, I. Exnar, P. Novak, J. Power Sources 101 (2001) 177.
[14] D. Goers, M. Holzapfel, W. Scheifele, E. Lehmann, P. Vontobel, J. Power Sources 130 (2004) 221.
[15] G.V. Riley, D.S. Hussey, D.L. Jacobson, ECS Trans. 25 (2010) 75.
[16] L.G. Butler, B. Schillinger, K. Ham, T.A. Dobbins, P. Liu, J.J. Vajo, Nucl. Instrum. Methods Phys. Res., Sect. A 651 (2011) 320.
[17] J.B. Siegel, X. Lin, A.G. Stefanopoulou, D.S. Hussey, D.L. Jacobson, D. Gorsich, J. Electrochem. Soc. 158 (2011) A523.
[18] T.A. Trabold, J.P., Owejan, J.J., Gagliardo, D.L., Jacobson, D.S., Hussey, M. Arif, in: W. Vielstich, H. A. Gasteiger, H. Yokokawa (Eds.), Handbook of Fuel Cells: Advances in Electrocatalysis, Materials, Diagnostics and Durability, vol. 6, John Wiley & Sons, Chichester, U.K., 2009.
[19] D.S. Hussey, D.L. Jacobson, M. Arif, K.J. Coakley, D.F. Vecchia, ASME Fuel Cells 2007 conference proceedings, New York, USA, June 18–20 2007.
[20] D.S. Hussey, D.L. Jacobson, in: U. Pasaogullari, C.Y. Wang (Eds.), Modern Aspects of Electrochemistry, vol. 49, Springer Publishing, New York, 2010.
[21] Neutron News, vol. 3, No. 3, 1992, pp. 29–37.